

# A material genome approach towards exploration of Zn– and Cd– coordination complex polyester as dielectrics: Design, synthesis and characterization



Shamima Nasreen<sup>a,b</sup>, Gregory M. Treich<sup>b</sup>, Matthew L. Baczkowski<sup>b</sup>,  
Arun K. Mannodi- Kanakkithodi<sup>c</sup>, Aaron Baldwin<sup>b</sup>, Sydney K. Scheirey<sup>a</sup>, Yang Cao<sup>d</sup>,  
Ramamurthy Ramprasad<sup>c</sup>, Gregory A. Sotzing<sup>a,\*</sup>

<sup>a</sup> Department of Chemistry, University of Connecticut, 55 N Eagleville Rd, Storrs, CT, 06269, United States

<sup>b</sup> Polymer Program, University of Connecticut, 97 N Eagleville Rd, Storrs, CT, 06269, United States

<sup>c</sup> Department of Materials Science and Engineering, University of Connecticut, 97 North Eagleville Rd, Storrs, CT, 06269, United States

<sup>d</sup> Department of Electrical and Computer Engineering, University of Connecticut, 97 North Eagleville Road, Storrs, CT, 06269, United States

## HIGHLIGHTS

- Series of coordination complex polyesters containing Zn and Cd metals are synthesized and characterized.
- Density Functional Theory is implemented for their electronic, spectroscopic and dielectric property evaluation.
- Dielectric constant is controlled by the metal identity/concentration, coordination environment and methylene spacer.
- Band gaps exceed that of their oxides and high to moderate dielectric constants are found with low dielectric loss.
- Strong correlation between the calculation and experimentation validates the goal of Materials Genome Initiative.

## ARTICLE INFO

### Keywords:

Dielectric  
Metal-polyester  
Band gap  
DFT  
Material genome

## ABSTRACT

Advances in materials can be achieved once we understand their property well. In this study, a series of zinc and cadmium aliphatic polyesters with varying numbers of methylene spacer(s), 1 to 8, are synthesized and characterized to understand their features, which control their dielectric properties. The rational co-design of these materials is adopted by Density Functional Theory (DFT) computations of local structural features, and physical properties as dielectric constant and band gap energies. Synthesized polyesters of zinc and cadmium exhibit high band gap energies, > 5 eV, with the dielectric constant from ca. 4.69–3.61 and ca. 6.61–4.01, respectively; with metal volume fractions ca. 3–12% experimentally, which supports the DFT computations strongly to behave as a good dielectric material. These initial studies give insight into the potential advantages and expansion of the chemical design space for developing new dielectrics and provide valuable validation and feedback to enrich Material Genome Initiative.

## 1. Introduction

The vastness of the polymer chemical universe makes it impractical to synthesize and test a significant number of candidates, whereas the modeling of several thousands may be possible using state-of-the-art computational resources and accurate computational techniques based on quantum mechanics. Indeed, approaches that involve accessing new chemical spaces through experiments guided by computations—referred to as *rational co-design* (Fig. 1)—are increasingly being employed

today, in order to reduce experimental cost and accelerate the material's design process [1]. This design philosophy is in the spirit of the Materials Genome Initiative [2], which was announced by the United States government, “to discover, manufacture and deploy advanced materials twice as fast, at a fraction of the cost”. As a result of this initiative, the last few years have seen several glittering examples of successful materials discovery that would be unlikely via standalone experiments, none more so than the design of novel polymeric dielectric materials [1,3–5].

\* Corresponding author.

E-mail address: [g.sotzing@uconn.edu](mailto:g.sotzing@uconn.edu) (G.A. Sotzing).

<https://doi.org/10.1016/j.polymer.2018.10.017>

Received 21 June 2018; Received in revised form 4 October 2018; Accepted 7 October 2018

Available online 09 October 2018

0032-3861/ © 2018 Published by Elsevier Ltd.

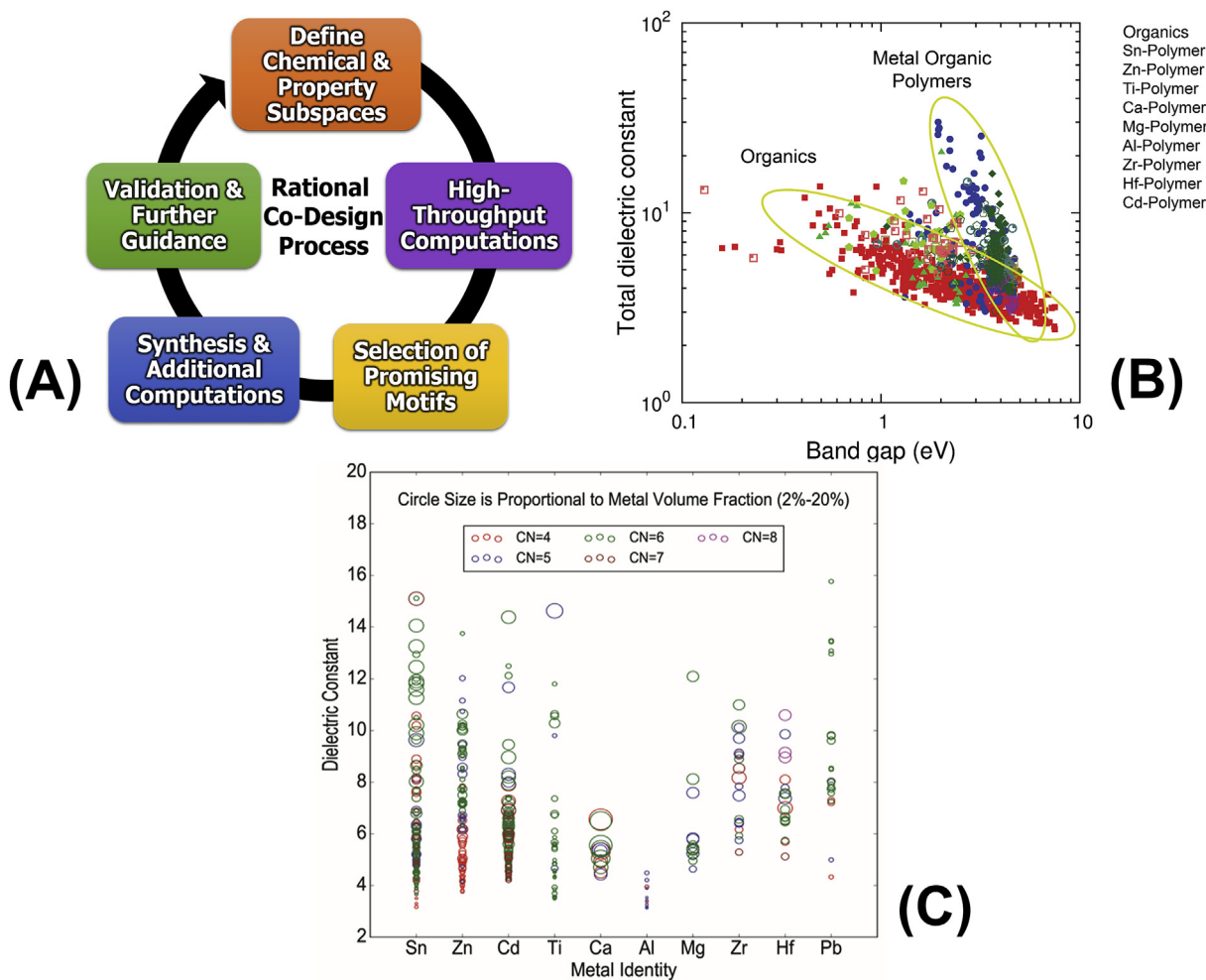


**Fig. 1.** (Top Left) (A) The primary steps involved in the rational co-design process. (Top Right) (B) Dataset of total dielectric constant as a function of band gap energy for over 1000 organic and metal containing organic polymers generated by DFT as a guidance for synthetic efforts. Reproduced with permission from Ref. [1], Copyright (2016) John Wiley & Sons, Inc. (Bottom) (C) Fingerprint-property correlation showing the dependence of dielectric constant on metal identity, metal volume fraction, and coordination number. Circle sizes correlate with the metal volume fraction (which ranges from 2% to 20%) whereas different colors correspond to different metal coordination numbers (which vary from 4 to 8). Reprinted (adapted) with permission from Ref. [6]. Copyright (2017) American Chemical Society. (For interpretation of the references to color in this figure legend, the reader is referred to the Web version of this article.)

Dielectric materials have the capability to polarize their atoms from an equilibrium position, under an applied electrical field, making them useful in applications such as capacitors, transistors, transformers, photovoltaics and photonics [7,8]. The use of inorganic ceramics as dielectric materials is a common practice due to their high dielectric constants, many in the thousands, which have been widely used in common electronic equipment, such as multilayer ceramic capacitors (MLCC) for the last few decades [9]. Various low temperature cofired ceramics (LTCC) have been developed with dielectric constants ( $\epsilon$ ) of 4–9 for use in three dimensional wiring circuit boards [10]. Recently, novel LTCCs with low dissipation have been developed; however, they exhibit lower dielectric constants as compared to common ceramic materials, which generally have high dielectric constants, suffer from high loss, and non-graceful failure modes [10,11].

Organic polyimides, polythioureas, polyurethanes and polyureas have also been recently studied for dielectric applications. They have their own advantages, such as easy processing and low dielectric loss, as well as disadvantages such as moderate to low dielectric constants with thermal limitations [12–14].

Apart from inorganic and organic polymers, numerous works have been carried out to develop dielectric materials with composite materials to enhance the dielectric constant [15–20]. Zinc oxide (ZnO) containing polyvinylidene fluoride (PVDF) nanocomposites are found

to have increased permittivity ( $\epsilon \approx 7.5$  to 15.5), with increasing amounts of ZnO content (1–6%), and decreased loss ( $\tan \delta \approx 0.75$  to 0.002), with decreases in frequency (0.12 kHz–100 kHz) due to orientational polarization [21]. These composites also increase their permittivity with increases in temperature (300–500 K) due to ion diffusion [21]. Other ZnO/polymer composite systems exhibit similar results to the PVDF composites, such as ZnO/Polyaryletherketone (PAEK) [22], ZnO/polyurethane [23] and nanosized ZnO/LDPE [24].

Pure zinc oxide (ZnO) crystals have a dielectric constant ca. 8.5 at 100 kHz [25] and a band gap of 3.37 eV [26]. Cadmium oxide (CdO) is a well-known n-type semiconductor metal oxide with a large refractive index ( $n_0 = 2.49$ ) [27] corresponding to an electronic dielectric constant of 6.2 using a result of the Maxwell equation, equation (1), and an optical band gap of 2.28 eV [28].

$$n_0 = \sqrt{\epsilon_{elec}} \quad (1)$$

Despite having high dielectric constants for metal oxides, CdO and ZnO have low band gap energies, which limit their application in high band gap materials. Moreover, inorganic aggregation is a common phenomenon, which makes them difficult to use as dielectrics due to their high dielectric loss under applied electric field and non-graceful aging mode [29]. Generally, it is a challenge to have high dielectric constant and low dielectric loss, while maintaining high band gap

energy, simultaneously.

Using high-throughput computational screening, followed by targeted synthesis and further in-depth computations, unexplored polymer classes (for eg., Sn-polyesters) were discovered as possible candidates for dielectric materials; this was recently reviewed [1]. As a part of this work, we generated a computational dataset of more than one thousand polymers and related materials, which is shown in the form of a plot between band gap and dielectric constant in Fig. 1 (B). It is evident that the metal containing polymers display much higher dielectric constant values for a given large band gap, as compared with pure organics. Therefore, recent computational studies have shown that by incorporating metal atoms into the polymer backbone through coordination bonds, dispersion difficulties of the aggregated nanoparticles in inorganic nanocomposite systems have been eliminated [30,31]. The rationale behind considering metal-oxygen bond in the polymer backbone is due to their dipolar and ionic contributions to dielectric properties, which occurs by increasing the difference in electronegativity between the metal-oxygen bonds. An initial exploration of organometallic polymers and compounds with group 14 elements, such as Si, Ge, Sn and Pb were examined using high-throughput density functional theory (DFT) calculations (the term high-throughput implying the use of a large number of computational resources on a large number of materials over an extended period of time) [1,5,6,32]. These calculations showed that an ester linkage to a tin atom was a favorable way to bind the metal into the polymer backbone, as it provides an increased atomic polarization, as well as increased dipole interactions. Various Sn-polyester systems were synthesized, studied and found to be promising materials with high dielectric constants ( $\epsilon \approx 5.3$ – $6.6$ ), low losses ( $\leq 2\%$ ), high band gap energies ( $E_g \approx 4$ ) and elevated operational temperatures ( $\approx 250^\circ\text{C}$ ), while correlating well with computational predictions [1,30]. The effect of structural morphology on electrical properties was controlled by blending and copolymerizing the Sn-polyesters [33]. Later, other metals have been investigated, and a large class of computational dataset have been developed, shown in the 4D plot in Fig. 1 (C), where dielectric constant is shown as a function of metal identity, metal concentration and coordination environment around the central metal atom [6]. This fingerprint–property correlation shows the importance of the metal concentration, metal coordination environment, and identity of its surrounding atoms in determining the dielectric constant. Different color distinguishes between coordination numbers and the size of the circle is proportional to the metal concentration. The later represents the metal volume fraction to the total crystalline volume of the polymer, as estimated from its computationally obtained crystal structure, ranged from the lower limit of  $\sim 2\%$  to a high of  $\sim 20\%$ . The circle size does not uniformly raise with an increase in dielectric constant, and at the same time the highest dielectric constant found for the system with 6-fold metal-oxygen coordination. It was also observed that certain polymers containing Zn, and Cd display dielectric constant  $> 5$ , even with low metal volume fractions of 2–10%. This important insight implies that it is possible to achieve increased dielectric constants of metal containing polymers without high concentration of metal content. Fig. 1C can serve as a valuable chart for the optimal window of metal atom, coordination number and metal content needed in a polymer backbone for a desired dielectric constant. It is to be noted that for each of these polymer repeat units, the structure prediction algorithm yielded several competing low energy structures, leading to a whole range of computed dielectric constants [6].

Therefore, in this study, the tin (Sn) system was replaced with the more electro-positive transition metals; zinc, a 3d block transition metal (Zn,  $[\text{Ar}]4s^23d^{10}$ ), and cadmium, a 4d block transition metal (Cd,  $[\text{Kr}]5s^24d^{10}$ ) with modified synthetic scheme. The goal of this study was multi-fold. Firstly, to explore the chemical space from the Periodic Table for feasible dielectric synthesis, so that we can understand their structure-property relationship from a broader perspective. It will help advance the material development, which is more prone to academic in

reason. Secondly, to narrow down the reasoning, it will be beneficial if we can synthesize new dielectrics, which can approach the dielectric constants of their corresponding metal oxides, without the downfalls of aggregation and high dielectric loss, while increasing their band gaps through the incorporation of a non-polar aliphatic spacers in the backbone. Also, to understand the mechanism of ionic, electronic and total dielectric constant contribution, along with the effect of metal identity, their concentration and coordination environment using high throughput DFT screening was done. Lastly, having late transition metals like Zn is cost effective, compared to the traditional synthetic organic polymers, which requires additional processing costs. However, Cd is slightly expensive; though the reason of using Cd is to have a comparative picture with the Zn counterpart.

## 2. Experimental section

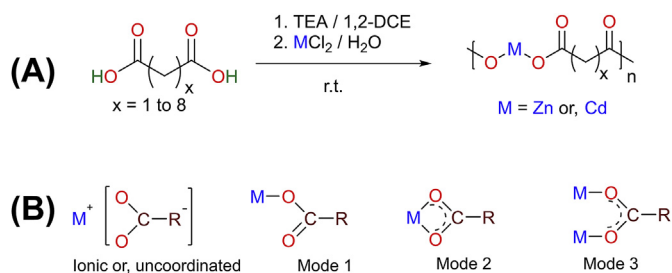
### 2.1. Calculation methodology

Density functional theory (DFT) [34] as implemented in the Vienna ab initio simulation package (VASP) [35] is the computational methodology used here. The total energies of the different structural models considered for the Zn- and Cd-systems were obtained using the generalized gradient approximation (GGA) functional associated with vdW-DF2 [36], i.e., refitted Perdew-Wang 86 (rPW86) [37]. The inclusion of the DF2 vdW correction [38] is necessary to explicitly take the weak interactions between adjoining polyester chains into account. For carbon, oxygen, hydrogen, zinc and cadmium, the following valence states were used respectively:  $2s^22p^2$ ,  $2s^22p^4$ ,  $1s^1$ ,  $3d^{10}4s^2$  and  $4d^{10}5s^2$ . Monkhorst–Pack k-point meshes [39] with a spacing of  $0.25 \text{ \AA}^{-1}$  were used for integrations over the Brillouin zones of the models. The plane wave kinetic energy cutoff was chosen to be 400 eV, and the atoms and unit cell parameters were simultaneously relaxed until the residual forces were smaller than  $0.01 \text{ eV \AA}^{-1}$ .

### 2.2. Materials and synthesis

$\text{CdCl}_2 \cdot 2.5\text{H}_2\text{O}$  (99%) and  $\text{ZnCl}_2$  (98%) were procured from Acros Organic. Triethylamine (99%) was purchased from Fisher Scientific. Malonic acid (99%), Succinic acid (99%), Glutaric acid (99%), Adipic Acid (99%), Pimelic acid (98%), Suberic acid (99%), Azelaic acid (98%), Sebacic acid (98%), Trifluoroacetic acid (99.5%) and 1,2-Dichloroethane 99.8+ % were procured from Acros Organic. Deionized water was collected from the Millipore purification system. Acetic acid-d4 (99.5%) was purchased from Cambridge Isotope laboratories, Inc. All commercially available chemicals and solvents were of reagent grade and were used as received without further purification. Quartz glass slides ( $3'' \times 1'' \times 1 \text{ mm}$ ) were procured from Ted Pella, Inc.

Several synthetic routes have been proposed in the literature for various Zn(II)- and Cd(II)-systems coordinated into the metal organic polymeric framework [27,40–47]. Here, a series of Zn(II) and Cd(II) aliphatic coordination complex polyesters were synthesized using a two-phase interfacial reaction as shown in Scheme 1A. Two sets of reactions were designed, one for zinc polymers and the other with zinc replaced by cadmium. Diacids ranging from 1 to 8  $-\text{CH}_2-$  spacers were taken in stoichiometric ratios in 1,2-dichloroethane (1,2-DCE) and then deprotonated with triethylamine. For the synthesis of poly (zinc malonate) Z1 1.4056 g (10.31 mmol) of  $\text{ZnCl}_2$  was dissolved in 18 mL of deionized water (DI) in a round bottomed flask. To a second flask, 1.1105 g (10.67 mmol) of malonic acid ( $\text{C}_3\text{H}_4\text{O}_4$ ) and 2.2124 g (21.86 mmol) of trimethylamine (TEA) were added in 20 mL 1,2-dichloroethane (1,2-DCE) and stirred until dissolution. The aqueous phase was then added slowly to the organic phase and allowed to react until precipitation occurred under ambient conditions. The precipitate was then filtered and washed with 100 mL of a 1:1 mixture of water and 1,2-DCE and dried *in vacuo* (30 in. Hg) at  $80^\circ\text{C}$  for 24 h. Yield: 0.890 g, 53%.  $^1\text{H}$  NMR (400 MHz, acetic acid-d4,  $\delta$ ): 3.53 (d,  $J = 6.1\text{Hz}$ , 2H).



**Scheme 1.** (A) General reaction scheme for the Zn- and Cd-systems with different di-acids. (B) Possible modes of interaction between carboxylate group ( $\text{COO}^-$ ) and metal, M; ionic or uncoordinated form (left), unidentate coordination (Mode 1), bidentate bridging coordination (Mode 2) and bidentate chelating coordination (Mode 3).

FTIR (ATR):  $\nu = 1525$  (vs;  $\nu_{\text{as}}(\text{C}=\text{O})$ ), 1443 (vs), 1389 (vs), 1311 (m), 1247 (s), 1203 (w), 970 (w), 957 (s), 901 (m), 804 (s), 709 (vs), 590 (m), 549 (w),  $431 \text{ cm}^{-1}$  (w);  $M_n$  ( $^1\text{H NMR}$ ):  $4.8 \times 10^4 \text{ g mol}^{-1}$ .

Similarly, **Z2-Z8** and **C1-C8** are synthesized and reported in supporting information. Polymer systems were named as **Z1** to **Z8** for Zn (II)-coordination polyester(s) and **C1** to **C8** for Cd(II)-coordination polyesters(s), respectively; where the digit indicates the number of methylene spacers in the various diacids.

### 2.3. General characterization

Fourier Transform Infrared (FTIR) spectra were collected on powder samples using a Nicolet Magna 560 FTIR spectrometer with a Specac Quest Diamond Attenuated Total Reflectance (ATR) accessory (resolution  $0.35 \text{ cm}^{-1}$ ) with 32 scans and are reported in wavenumbers ( $\text{cm}^{-1}$ ) from 400 to  $4000 \text{ cm}^{-1}$  (see supporting information). Thermogravimetric Analysis (TGA) was performed using a TA instrument's TGA Q500 with a heating rate of  $10 \text{ }^\circ\text{C}$  per minute from  $25 \text{ }^\circ\text{C}$  to  $600 \text{ }^\circ\text{C}$  under nitrogen atmosphere. Differential Scanning Calorimetry (DSC) was performed on a TA instrument's DSC Q20 with a first heating cycle rate of  $30 \text{ }^\circ\text{C}$  per minute, a cooling cycle of  $30 \text{ }^\circ\text{C min}^{-1}$  followed by a second heating cycle of  $10 \text{ }^\circ\text{C}$  per minute. X-ray Diffraction (XRD) patterns were collected on a Bruker D2 Phaser with  $\text{Cu-K}\alpha$  ( $\lambda = 1.54184 \text{ \AA}$ ) source beam with an accelerating voltage of 30 kV, and cathode current of 10 mA. The data were collected in the range of  $5$  to  $70^\circ 2\theta$  values with a step size of  $0.02^\circ$ . Solution  $^1\text{H NMR}$  (400 MHz and 300 MHz) was performed using a Bruker AVANCE III 400 and AVANCE 300 high resolution digital NMR spectrometer with acetic acid- $d_4$ . Chemical shifts are reported in parts per million (ppm,  $\delta$ ) versus the chemical shift of the residual acetic acid peak being labeled at 2.04 ppm. Splitting patterns are reported as singlet (s), doublet (d), triplet (t), multiplet (m), etc. Density measurements were conducted by pressing a 1-inch diameter pellet using a Carver Laboratory Press with a pressure of 15,000 pound-force per square inch ( $1 \times 10^5 \text{ kPa}$ ) via a hydraulic press at room temperature, and measuring the thickness and mass, and calculating the volume,  $V$ , of the pellet and using the equation  $V = \pi r^2 h$ , where  $\pi = 3.142$ ,  $r$  = radius of the pellet. The sample thickness was determined using a thickness gauge (Model LE1000-2, Measure It All) as the average of five samples. Density was then calculated from the measured volume and mass taken of the polymer sample. Metal volume percentage was determined by relating the density of the pellet with the metal weight fraction, as determined by  $^1\text{H NMR}$  and compared to a theoretical metal volume percentage calculated by the covalent volumes inside the unit cell by DFT.

### 2.4. Electrical characterization

All pellets that were made were dried in a vacuum oven for 2 h before taking the final electrical measurements. Frequency-dependent capacitance and dissipation factors ( $\tan \delta$ ) were measured using an

Agilent 4284A Precision LCR meter sweeping from 20 Hz to 1 MHz of a pressed pellet sandwiched in between two silicone electrodes, and the effect of water on electrical properties was monitored in different temperatures in the same LCR meter connected with an insulated oven purged with nitrogen. Conductivity is estimated by using the equation  $\tan \delta = \sigma / 2\pi f \epsilon \epsilon_0$ ; where  $\sigma$  stands for the conductivity,  $f$  is the corresponding frequency in Hz,  $\epsilon$  is the measured dielectric constant and  $\epsilon_0$  is the vacuum permittivity ( $\sim 8.85 \times 10^{-12} \text{ F/m}$ ). A Cary 5000 UV-Vis-NIR was used to measure polymer band gaps. 3 wt/wt.% solution of polymers with TFA were casted onto a quartz glass slide (Ted Pella, Inc.,  $3'' \times 1'' \times 1 \text{ mm}$ ) and dried *in vacuo* at  $115 \text{ }^\circ\text{C}$  to remove residual solvent. The UV-Vis spectrum was recorded from 750 to 190 nm and the onset wavelengths of absorption,  $\lambda_{\text{onset}}$ , were determined to calculate band gap energies in eV using Planck's equation (see supporting information).

## 3. Results and discussion

### 3.1. General characteristics

All of the synthesized polymers were white in color and did not show any degradation in ambient conditions. It was found that both the reactivity and yields were higher with the transition  $3d^{10}$  metal Zn(II) than with the  $4d^{10}$  metal Cd(II), as shown in Fig. S1. Polymers exhibited solubility in both acetic acid and trifluoroacetic acid. When dissolved in acetic acid, there was no evidence of chain end degradation, indicating that the polymers were stable in the acidic solution. Samples were prepared for  $^1\text{H NMR}$  with acetic acid- $d_4$  as the solvent. Number average molecular weights,  $M_n$ , were calculated from the  $^1\text{H NMR}$ . The molecular weights ranged from ca.  $4.4\text{--}8.7 \times 10^4 \text{ g mol}^{-1}$  for Zn(II)-polyesters and ca.  $5.2\text{--}8.8 \times 10^4 \text{ g mol}^{-1}$  for Cd(II)-polyesters.  $^1\text{H NMR}$  spectra shown for **Z3** and **C4** in Fig. S12 and Fig. S13.

### 3.2. DFT features and structural confirmation

In order to perform DFT computations on these polymers, it was necessary to determine the ground state crystal structures for each. The Minima Hopping algorithm [48,49] was used to explore low energy regions of configurational space in the Zn(II)- and Cd(II)-systems; unknown structural motifs could be readily obtained by starting from any initial structure, as this method employs zero constraints on atomic positions or cell shapes. Structural motifs were predicted for each of the Zn(II)- and Cd(II)-systems, from 1  $-\text{CH}_2-$  to 8  $-\text{CH}_2-$  spacers, of which 8 to 10 low energy structures were selected for each. In general, it was observed from the obtained structures that the Zn/Cd atoms exist in either a 4-fold or a 6-fold coordination environment. The metal atoms link together  $-\text{COO}-$  groups of different chains to either form two-dimensional or three-dimensional networks; three unique kinds of motifs thus seen across the different Zn- and Cd-systems (referred to as motifs  $\alpha$ ,  $\beta$  and  $\gamma$ ) are shown in Fig. 2.

Once the most stable structures were predicted for any given composition of the Zn(II)- or Cd(II)-coordination polyesters, the dielectric constants were calculated for each of them within the Density Functional Perturbation Theory (DFPT) [50] formalism as implemented in Vienna ab-initio Software Package (VASP). Dielectric tensors corresponding to the electronic and ionic contributions to the dielectric constant were obtained from the DFPT computation. The reported (electronic and ionic) dielectric constant values were the traces of these tensors, while the total dielectric constant values were obtained as the sum of the two components. The dielectric constant was seen to depend on the structural motif, and the final values reported for each system was an average of the overall low energy structures. Furthermore, the FTIR spectra for the structures were also computed for a direct comparison with the experimentally obtained spectra (see supporting information). For any given structural motif, FTIR intensities for different frequency modes were calculated utilizing the DFT computations, given

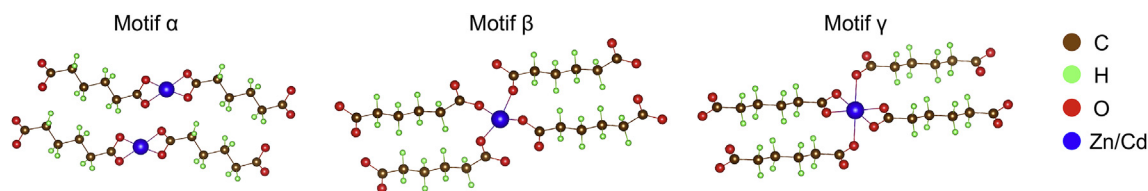


**Fig. 2.** Fraction of the three kinds of polymer motifs are shown for the Zn– and Cd–systems, illustrating the double chain configuration and coordination geometry. Motif  $\alpha$  shows a 2D motif for a 4-fold coordination, Motif  $\beta$  shows a 3D motif with a 4-fold coordination, and Motif  $\gamma$  shows a 3D motif with a 6-fold coordination of metal.

as a function of Born effective charge tensors and phonon mode eigenvectors for all the atoms in system [51].

In the experimental FTIR spectra, Figs. S2–S5 for Z1–Z8 and C1–C8, the expected strong absorption bands were observed for C–O, and in all cases, were found to be in the range of 1525–1560  $\text{cm}^{-1}$ , while symmetric bridging and non-bridging occurred at 1410–1453  $\text{cm}^{-1}$  and 1322–1398  $\text{cm}^{-1}$ , respectively [52]. Uncoordinated carboxylic acid (C–O) typically shows peaks around 1725–1700  $\text{cm}^{-1}$ , and was not found in any spectra, confirming that nearly all carboxylic acids were coordinated to metals. The sharp peaks at the region 454–411  $\text{cm}^{-1}$  were attributed to the Zn–O bond [53], while the peaks at 584–517  $\text{cm}^{-1}$  were associated with the Cd–O bond [54]. These absorption bands were well anticipated in the computed IR; however, slight shifting of these peaks were observed in experimentation, since these structures had been considered as their perfectly crystalline form in zero Kelvin. In Scheme 1B, four different kinds of interactions are shown for metal to oxygen bonding. A general trend for symmetric and asymmetric band separation values can be summarized as: uncoordinated acid > unidentate coordination > bi-dentate (bridging > chelating) coordination [55]. The FTIR spectral analysis showed (Table S1) the presence of a bidentate bridging or -inter chain motif (Mode 3) and a chelation (Mode 2) or -intra chain motif mode of interaction between the metal carboxylate groups for all of the Zn(II)- and Cd(II)-coordination polymers [56,57]. An increase in the intensity of the C–H stretching band was found in the region of 2850–2950  $\text{cm}^{-1}$  as the number of  $-\text{CH}_2-$  spacers increased from Z1 to Z8 and C1 to C8 due to the  $\text{sp}^3$  hybridized methylene unit(s) (see supporting information). With the incorporation of more  $-\text{CH}_2-$  spacers, a three-dimensional network was possible due to the flexibility of the aliphatic chain within the coordination environment. This network was also found in the DFT modeling as 4-fold and 6-fold coordination within the possible 2D ( $\alpha$  motif) or 3D ( $\beta$  and/or,  $\gamma$  motifs) complex network [30,56,58,59]. Zn(II)-polyesters favored an orientation of 4-fold coordination, whereas, Cd(II)-polyesters showed a preference to a 6-fold coordination environment. The larger size of the metal center of 4d-block Cd(II), compared to that of 3d-block Zn(II), enables it to bind to this additional ligand in a 6-fold coordination environment [60].

### 3.3. Dielectric spectroscopy

A comparison of the experimental dielectric properties of these sixteen polymeric systems to their theoretical calculations was done by testing the polymers as pressed pellets at ambient conditions of 25 °C in air. Pellets were dried *in vacuo* (30 in. Hg) at 100 °C overnight to ensure desorption of any water molecules. All measurements were done immediately after drying. To determine their dielectric constants ( $\epsilon$ ) and dissipation factors ( $\tan \delta$ ), frequency domain spectroscopy from 20 to 1 MHz was carried out, as shown in Fig. 3A and C for the Zn(II)-polyesters and Fig. 3B and D for the Cd(II)-polyesters. For dielectric spectroscopy measurements, pressed pellets were sandwiched between two conductive silicone electrodes and compressed to ensure no air was present between the electrodes and the pellet. The dielectric constant was calculated from the measured capacitance by equation (2), where

$$\epsilon = Cd / \epsilon_0 A \quad (2)$$

$\epsilon$  is the relative dielectric constant of the capacitor,  $C$  is the capacitance (Farads),  $d$  is the thickness of the sample (m),  $\epsilon_0$  is the permittivity of free space ( $8.854 \times 10^{-12}$  F/m) and  $A$  is the capacitor electrode surface area ( $\text{m}^2$ ). The ZnO (Sigma Aldrich, ACS, 99%) and CdO (Sigma Aldrich, trace metal, 99.5%) were collected, and their pressed pellets were tested for dielectric spectroscopy. They were then compared with the dielectric properties of synthesized polymers. Of the eight Zn(II)-polyesters systems, the highest dielectric constant at 1 kHz was found for Z1 with ca. 4.69, with loss ca. 2%, and the lowest dielectric constant was found for Z8 ca. 3.61, with loss ca. 4%. The remaining zinc systems, Z2–Z7, exhibited dielectric constants that lied between the values found for Z1 and Z8. Dielectric constant from ZnO pellets was found as ca. 8.61 with a high loss ca. 25%. The calculated dielectric constant values for the polymers shown in Table 1 and Table 2 were from the best-fit FTIR plots, and the lowest energy structures were predicted to have slightly higher values than observed in the experimental results. It was observed that the dielectric constants for Zn(II)-polyesters exhibited a plateau during the early frequencies at 100 Hz, and there was no significant decrease on their values on higher frequencies. Similarly, dissipation factors ( $\tan \delta$ ) were low ( $\approx 0.005$ – $0.042$ ), with low frequency dispersion for Zn(II)-polyesters, unlike the high dissipation factors and high frequency dispersion for ZnO. Similar trends also observed in the Cd(II)-polyesters, with overall higher dielectric constants. C1 showed the highest dielectric constant ca. 6.61 at 1 kHz and was in close agreement with the calculated value, which was found to be ca. 6.90. These values for C1 showed close resemblance with corresponding CdO, with a measured value found as ca. 6.95 at 1 kHz. It is to be noted that C1 showed much improvement in its dissipation factor with relatively lower loss as ca. 4%, compared with CdO as ca. 27% at 1 kHz. The lowest dielectric constant of the Cd(II)-polyesters was found for C8, ca. 3.97, with low loss, 0.5%, at 1 kHz. However, the rest of the cadmium polymers, C2 to C7, exhibited intermediate electrical properties with respect to C1 and C8. On the other hand, dielectric constants gradually decreased as a function of increasing applied frequency, and reached a plateau at 10 kHz for C1–C4 polymers and also low frequency dispersion was observed for C5–C8 polymers.

Dissipation factors decrease with increasing frequencies, which is typical for most dielectric material due to the polarization and conduction loss [61]. Initial high loss can be attributed to the mobile charges within the polymers [61], which was much lower than the corresponding CdO. Similarly, most of the calculated values in the remaining systems matched the experimental findings quite well, as found in Table 2. The log-log plot in Fig. 3(E) and (F) show the estimation of the conductivity based on the dielectric loss factors, as determined by TDSS. In the frequency range tested, there is no clear indication for the onset of DC conduction loss. The upper bound of the conductivity for both materials was found to be  $\sim 10^{-11}$   $\text{Sm}^{-1}$ . As we have not observed the DC conduction plateau (towards 0 Hz), the true DC conduction could be lower.

It is also evident that the dielectric constant contribution is dependent on the polarization of the highly electropositive metal and electronegative oxygen bond, hence the overall dielectric constant decreases as more non-polar  $-\text{CH}_2-$  spacers enter the polymer backbone,

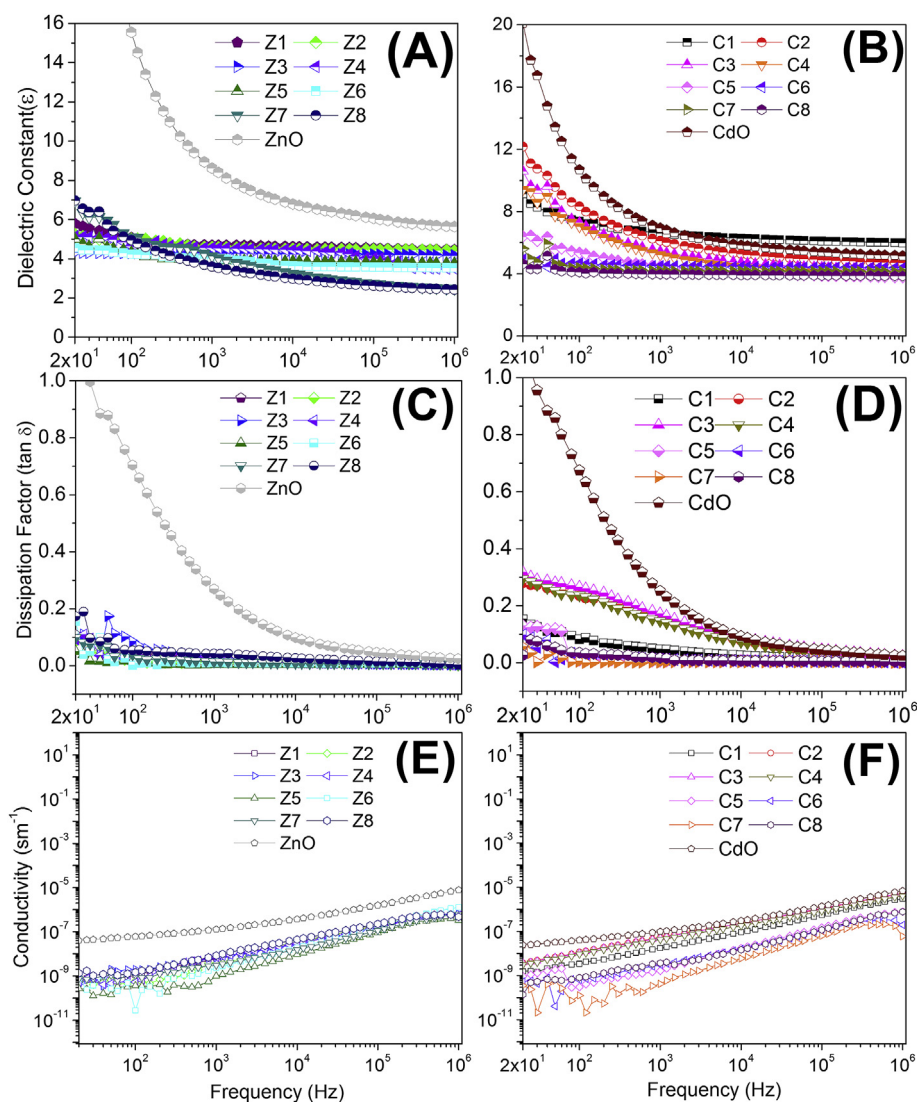


**Fig. 3.** (A) Dielectric constants, (C) corresponding dissipation factors, and (E) estimated upper bound of the conductivity for Zn(II)-polyester(s) and ZnO based on dielectric loss factor; (B) dielectric constants, (D) dissipation factor, and (F) estimated upper bound of the conductivity for Cd(II)-polyester(s) and CdO based on dielectric loss factor over the frequency range 20–1 M Hz at room temperature.

**Table 1**

Measured dielectric constants ( $\epsilon_{\text{exp}}$ ), calculated total dielectric constants ( $\epsilon_{\text{calc}}$ ), measured dissipation factors ( $\tan \delta$ ), measured band gap energies ( $BG_{\text{exp}}$ ), and calculated band gap energies ( $BG_{\text{calc}}$ ), calculated metal volume fraction ( $MV_{\text{calc}}$ ) and measured metal volume fraction ( $MV_{\text{exp}}$ ) and calculated coordination numbers ( $CN_{\text{calc}}$ ) for Z1–Z8 polymers.

Zn(II) polymer(s)	Z1	Z2	Z3	Z4	Z5	Z6	Z7	Z8
$\epsilon_{\text{exp}}$ at 1 kHz (r.t.)	4.69	4.59	4.28	4.56	3.93	4.01	4.14	3.61
$\epsilon_{\text{calc}}$	5.05	4.94	4.70	5.55	4.16	4.28	4.02	4.85
$\tan \delta_{\text{exp}}$ at 1 kHz (r.t.)	0.023	0.014	0.027	0.021	0.005	0.010	0.013	0.042
$BG_{\text{exp}}$ (eV)	5.67	5.47	5.49	5.51	5.42	5.21	5.53	5.57
$BG_{\text{calc}}$ (eV)	6.38	6.89	6.36	6.31	6.53	6.19	6.41	6.35
$MV_{\text{calc}}$ (%)	9.51	8.23	7.05	6.16	5.50	4.62	4.42	4.24
$MV_{\text{exp}}$ (%)	8.84	7.57	6.01	6.98	5.28	4.17	4.01	3.29
$CN_{\text{calc}}$	4	4	4	4	4	4	4	6

causing a decrease in metal concentration within the unit cell. DFT generated electronic, ionic and total dielectric constant contribution of these metal containing polymeric system are shown in Fig. 4. It is found that the electronic dielectric constant contributions of these system are independent of the aliphatic chain length and the metal concentration

**Table 2**

Measured dielectric constants ( $\epsilon_{\text{exp}}$ ), calculated total dielectric constants ( $\epsilon_{\text{calc}}$ ), measured dissipation factors ( $\tan \delta$ ), measured band gap energies ( $BG_{\text{exp}}$ ), and calculated band gap energies ( $BG_{\text{calc}}$ ), calculated metal volume fraction ( $MV_{\text{calc}}$ ) and measured metal volume fraction ( $MV_{\text{exp}}$ ) and calculated coordination numbers ( $CN_{\text{calc}}$ ) for C1–C8 polymers.

Cd(II) polymer(s)	C1	C2	C3	C4	C5	C6	C7	C8
$\epsilon_{\text{exp}}$ at 1 kHz (r.t.)	6.61	6.13	5.43	5.22	4.47	4.50	4.19	4.01
$\epsilon_{\text{calc}}$	6.90	6.51	5.73	5.42	5.88	5.07	4.90	4.29
$\tan \delta_{\text{exp}}$ at 1 kHz (r.t.)	0.041	0.155	0.171	0.145	0.006	0.012	0.002	0.016
$BG_{\text{exp}}$ (eV)	5.49	5.55	5.41	5.50	5.52	5.81	5.47	5.54
$BG_{\text{calc}}$ (eV)	5.29	5.31	5.53	5.91	5.88	5.75	5.25	5.54
$MV_{\text{calc}}$ (%)	13.8	11.8	10.0	8.53	7.72	7.01	6.34	5.74
$MV_{\text{exp}}$ (%)	11.9	12.0	9.37	8.29	6.12	7.39	6.32	5.69
$CN_{\text{calc}}$	4	6	6	6	6	6	6	6

in the system. The ionic dielectric constant contribution of these metal systems is responsible for the trend in total calculated dielectric constants. Both the ionic and total dielectric constant trends followed the experimental values closely for each of the systems. So, it can be argued that the ionic nature of the metal-oxygen bond is responsible for

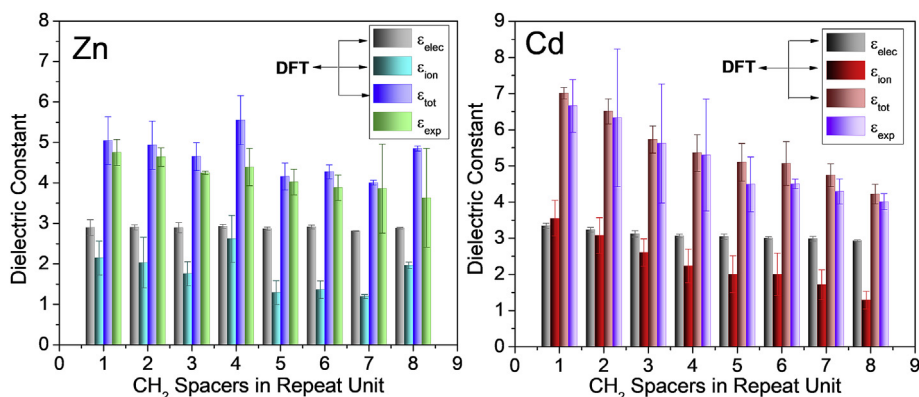


Fig. 4. Electronic, ionic and total dielectric constants contribution along with the averaged experimental dielectric constants with respect to methylene spacers in the polymer repeat unit for Zn(II)- and Cd(II)-polyesters.

controlling the ionic part of the dielectric constant. When the number of aliphatic non-ionic  $\text{CH}_2$  spacers are increasing within the unit cell, this affects the ionic polarization under applied electric field and hence, overall dielectric constant decreases.

This can be further explained by Fig. 5; where, this tendency can be correlated with both the calculated and experimental dielectric constants, and the calculated and experimental volume fraction that metals occupy within individual systems. An increase in the experimental metal volume fraction from 3.29 to 8.84% (DFT 4.24–9.51%) for Zn(II)-polyesters and 5.69–12.01% (DFT 5.74–13.80%) for Cd(II)-polyesters improves the dielectric constant when we decrease the repeat unit chain length by aliphatic spacers. It would be expected, as it can increase the ionic portion of the dielectric constant, hence increased ionic polarization. It is to be noted that Zn(II)-polyesters mostly adopted the 4-fold coordination environment by having metal-oxygen linkage, on the other hand, Cd(II)-polyesters mostly adopted 6-fold coordination, which is also summarized in Tables 1 and 2.

Overall both systems exhibited a trend where the systems containing an even number of methylene spacers were more likely to show a slightly higher dielectric constant than its adjacent odd spacers. This trend matched well with the slightly higher calculated total dielectric constants observed for all systems. The slight disparity between the calculated and experimental dielectric constant values may be because the calculated values were found for a specific lowest energy structural representation of the individual system; whereas, the experimental system may have a mixture of all the possible structures in the polymeric chain. Moreover, for 7 and 8 methylene spacers there is a high chance of chain entanglement and ring formation which might cause the slightly higher deviation from the calculated dielectric constant value, since calculated values are generated considering the linear

arrangement of the chains. Possible ring formation and chain entanglement due to the higher number of methylene spacers could adversely affect the molecular weight, structure and morphology of the polymer. As such, there can be an adverse effect to the dielectric properties due to the reduction in the overall polarizability, which depends on chain flexibility and orientation. Zn(II) being smaller than Cd(II) would have more propensity to ring closure. Further deviation in calculated vs. experimental results can be derived from the lower crystallinity in the prepared polymers vs. the polymers being calculated from a high crystalline structure.

### 3.4. Band gap and morphology

The band gap, or energy gap between the valence band and conduction band, can be considered a good indicator for a material to be an effective dielectric medium. The higher the gap, the more energy is required to promote the electrons from the highest occupied molecular orbital (HOMO) to the lowest unoccupied molecular orbital (LUMO) to behave as a conductor. Material containing a band gap of  $> 3$  eV is generally considered as suitable dielectric [62].

For these synthesized polymers, band gaps and crystal structures were also predicted in greater detail and with more accuracy using computations. The respective ground-state stable 3D structural arrangements of the polymers were determined, in which the bandgap was estimated using the Heyd–Scuseria–Ernzerhof (HSE) electronic exchange-correlation functional for purely crystalline representation, which offers more reliable results at sufficiently higher computational cost. While the calculated dielectric constants were found to range from 4 to 6, the bandgaps were seen to be greater than 5 eV for all metal systems. DFT-predicted ground-state structures are expected to be

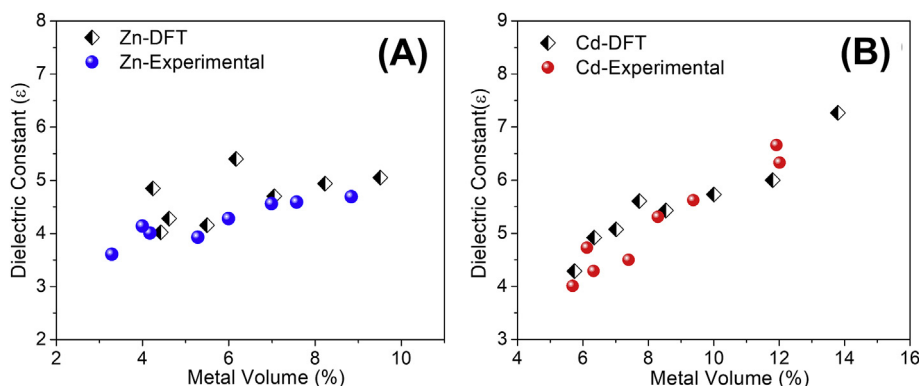


Fig. 5. Plots generated from the total dielectric constant by DFT and experimental average dielectric constant over the frequency range of 20–1 MHz as a function of DFT and experimental metal volume fraction (MVF) in percent for (A) Zn(II)- and (B) Cd(II)-polyesters, respectively.

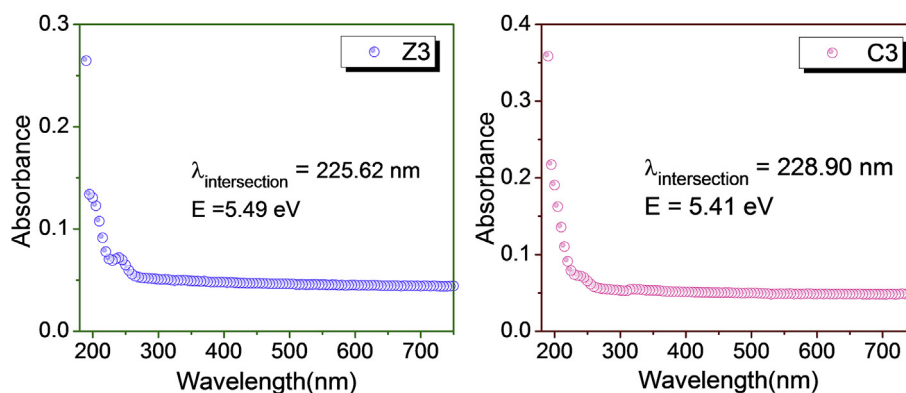


Fig. 6. Band gap energy of Z3 and C3 polymers from the onset of interband optical absorption from UV–Visible spectrum.

stable at room temperatures, as well, and thus, the computed values are expected to stand at higher temperatures as well with slight differences.

At higher field, electrons from the HOMO transfer to the LUMO, hence producing an impact ionization to behave as a conductor; which can be measured through the onset of interband optical absorption or excitation from the UV–vis spectrum [63,64]. Therefore, experimental optical band gap measurements were taken by scanning the UV–visible spectrum from 750 to 190 nm and measuring the wavelength at onset of interband optical absorption shown in Fig. 6 for Z3 and C3 polymers and rest of them are shown in Fig. S6.1 and Fig. S6.2. The energy band gap ( $E_g$ ) is calculated from Planck's relation (3), where  $h$  is the Planck's constant ( $4.136 \times 10^{-15}$  eV s) and  $c$  is the speed of light in vacuum ( $2.998 \times 10^{15}$  nm/s)

$$E_g = hc/\lambda_{\text{onset}} \quad (3)$$

High optical band gap values ranging from ca. 5.21–5.67 eV for Zn (II)-polyesters and ca. 5.49–5.81 eV for Cd(II)-polyesters were observed and listed with the calculated values in Table 1, and showed close resemblance with the DFT predicted values. However, Zn(II)-polyesters showed slightly lower experimental values when compared to the corresponding calculated band gap energies. Despite slight differences in the band gap values, which was anticipated for the semi-crystalline or amorphous nature of the polymer, the measured band gaps resembled nicely with the computations overall. Band gap energies of metal containing polymers exceeded the typical band gap energies of the corresponding oxides ( $\text{ZnO} \approx 3.37$  eV and  $\text{CdO} \approx 2.28$  eV), due to the incorporation of non-polar methylene spacers inside the structure. Moreover, dielectric constants remain high for metal containing polymers, simultaneously maintaining high band gap energies unlike organic polymers. The electropositive nature of the metal atom and their easy polarizability lead to large dipole moments within individual chain segments. Additionally, their soft nature of stretching and wagging vibrational modes imparts higher IR intensities, and hence, higher ionic contributions in their dielectric constant, which leads to high total dielectric constant without affecting the band gap as predicted [6]. Their averaged dielectric constants and band gaps are plotted in Fig. 7 (A) with a few known polymers—namely polyethylene (PE), polypropylene (PP) (dielectric constant  $\sim 2.2/2.2$  and bandgap  $\sim 7$  eV), and with other common commercially available organic polymers for comparison with the synthesized Zn and Cd containing polymers. For comparison, DFT generated complete data sets are also represented in Fig. 7 (B) for both organic and metal containing polymers. The promise from DFT data clearly reflected in reality for the sub space expansion with Zn and Cd containing polymers.

The effect of the number of methylene spacers per unit volume is evident in X-Ray Diffraction (XRD) patterns shown in Fig. S7. Both Zn (II)- and Cd(II)-polyesters exhibited a crystalline nature in their pattern with the exception of the C1, C2 and C3, which showed semi-crystalline nature. This exception suggests a random orientation in the coordinated

polymeric chain of C1, which appears to be more amorphous in nature when compared to C2 and C3 as the diffraction pattern shows a greater lack of crystallinity. A smaller aliphatic spacer in C1 might impart more intrinsic strain to arrange itself to form an extended polymeric chain in a more random fashion. Similarly, Z1 and Z2 showed lower crystallinity compared to other systems. Increasing the number of methylene spacers in the polymer repeat unit can be attributed with a fact of increasing the  $d$  spacing as shown in the XRD pattern, which is listed in Table S2 for the most intense peak of the pattern in both systems. The shifting of this peak as shown with an arrow in Fig. S7 for Z3–Z8 and C4–C8. It is also evident that Z3 followed a similar decreasing trend unlike C3, which was indicative of the semi-crystalline nature of its powder form.

### 3.5. Thermal performance

All polymers were tested for their onset of degradation ( $T_d$ ) via Thermogravimetric Analysis (TGA), as found in Table 3, and appearance of thermal transitions via DSC. No thermal transition was observed for all these systems as apparent as in Fig. S11 for Z3 and C3. It was found that the Zn(II)-polyesters were thermally more stable than the Cd (II)-polyesters, despite the low degradation of Z1.

C1–C5 polymers showed a tendency to absorb  $\sim 0.5\%$  water by wt. in 1 h if left in open atmosphere, as can be seen in Fig. S9 for C1. This phenomenon is evident in the FTIR spectrum in Fig. S4 (see supporting info.) and also by TGA shown in Fig. S8 for C4–C5 polymers. The Cd (II)-coordination polymers showed a greater tendency to absorb water than the Zn(II)-coordination polymers, which was due to the larger size of the metal center of Cd(II) ( $r \approx 0.95$  Å) compared to the Zn(II) ( $r \approx 0.74$  Å). That larger size allowed small water molecules to interact as bound water or loosely bound water in the crystal lattice. C1 and C2 showed initial weight loss at 104 °C and 161 °C, respectively, which might be associated with loosely bound water or free water. For the C3 system, initial weight loss was found at ca. 100 °C, which continued to increase until 210 °C. This could be explained by the initial loss of free water, which gradually started to eliminate loosely bound water above 100 °C and finally bound water up to ca. 210 °C, as the elimination of bound water molecules has been known to take place between 150 and 250 °C [65]. Similarly, for C4 and C5, ca. 2% weight loss could be associated with all three possible forms of water binding at 150–250 °C. In order to further understand if freely bound water was present in the Cd (II)- polyester(s), a cyclic thermo-gravimetric study was performed along with FTIR. The previously oven dried C1 sample was heated to 150 °C in the TGA analyzer under an inert atmosphere and held for 1 h at that temperature to remove any absorbed water. Approximately 5.5% of the weight loss was observed in the first cycle of the TGA run due to the absorbed water shown in Fig. S9, which was not found after a second heating cycle up to 150 °C under an inert nitrogen atmosphere. This process was run again with the same sample after allowing the sample to rest in the atmosphere for 1 h. This time, ca. 0.5% of water

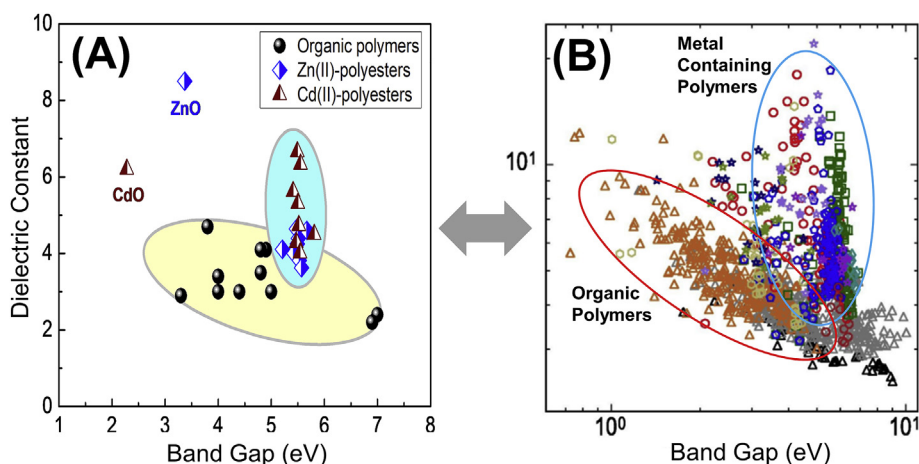


Fig. 7. (A) Experimental averaged dielectric constant as a function of band gap energy for metal oxides, metal containing polyesters, and several common commercially available organic polymers; (B) DFT generated dielectric constants and band gap energies of more than one thousand organics are shown in orange, gray and black symbols, and metal containing polymers are represented by the other colors, Reproduced from Ref. [32], Copyright (2017), with permission from Elsevier. (For interpretation of the references to color in this figure legend, the reader is referred to the Web version of this article.)

Table 3

Thermal data from TGA showing temperature at onset of degradation ( $T_d$ ) and temperature at 5% weight loss ( $T_{5\%}$ ) for Zn(II)- and Cd(II)-polyester(s).

Zn(II)-polyester(s)	Z1	Z2	Z3	Z4	Z5	Z6	Z7	Z8
$T_d$ (°C)	164	327	315	326	332	327	303	311
$T_{5\%}$ (°C)	215	419	360	370	355	361	345	333
Cd(II)-polyester(s)	C1	C2	C3	C4	C5	C6	C7	C8
$T_d$ (°C)	263	317	310	245	233	293	273	280
$T_{5\%}$ (°C)	271	196	210	279	296	328	293	301

was absorbed, indicating the hygroscopic nature of the C1 polymer. The appearance of  $-\text{OH}$  stretching as a broad band at  $3376\text{ cm}^{-1}$  in the FTIR before the thermal treatment is indicative of the absorbed moisture, which was absent after the thermal treatment showing in the inset of Fig. S9. The band at  $3519\text{ cm}^{-1}$  was assigned to hydrogen bonding due to the strongly bound water, which disappeared after heating to  $150\text{ }^\circ\text{C}$ .

It has been previously reported that the presence of water can significantly affect the dielectric properties of system [66]. The C5 system was chosen for further investigation to observe the effect of temperature on dielectric properties (Fig. S10) as it showed a lower average dielectric constant ca. 4.23. Temperature dependent dielectric spectroscopy was carried out on an LCR meter connected to a computer for measurement control and data analysis, which extended into an oven for temperature control in an inert atmosphere. The dielectric constant increased initially when it was treated from  $30\text{ }^\circ\text{C}$  to  $90\text{ }^\circ\text{C}$  due to the increased vibrational dipolar orientation, which subsequently caused the enhancement of charge carrier mobility [66,67]. Similarly, the dissipation factor also increased with the increase of temperature. After  $90\text{ }^\circ\text{C}$ , the dielectric constant decreased due to desorption of the dipolar water molecule from the system. The additional ligand, which was found to be bound water, to the Cd(II) center lead to an increase in the segmental dipole moment of the system. When the whole system was heated to an elevated  $150\text{ }^\circ\text{C}$ , removal of bound water decreased the total dipole moment leading to a lower dielectric constant.

#### 4. Conclusion

In summary, a rational co-design approach was successfully implemented for the targeted discovery of new polymeric dielectric materials. The use of transition metals in a polymer with aliphatic spacers allowed for dielectric constants close to the metal oxides to be reached, while drastically increasing the band gap energies with low dissipation factors. A series of Zn- and Cd-containing polyesters were computationally studied, and trends in their DFT-computed dielectric constants and band gaps are reported. The proposed structural models, as well as

the calculated spectroscopic, electronic and dielectric properties, strongly correlate with the experimental findings observed in both the Zn(II)- and Cd(II)- coordination complex polymeric systems and give confidence to future computations of other transition metals. The Cd(II)-polyesters have higher dielectric constants (ca. 6.61 to 4.01) compared to Zn(II)-polyesters counterparts (ca. 4.69 to 3.61), as was predicted by DFT. Moreover, they showed significant improvement over energy loss with less than 0.5–4% at maximum at 1 kHz. Additionally, band gap energies were observed to be on  $5.51 \pm 0.121\text{ eV}$  for all sixteen systems, which exceeds the typical optical band gap energies of ZnO and more than doubles that of CdO. This study revealed that the identity of the metal, its character, the concentration of the metals and the coordination environment of the metal atoms are among the crucial factors for behaving as a dielectric. The desired dielectric constant can be achieved by the optimal mixture of these factors. The close agreement between calculated and experimental findings in our work can serve as a starting point for further research directed towards the expansion of chemical space for other metals and linker systems. This “computations  $\rightarrow$  experiments  $\rightarrow$  computations” synergistic loop was successfully pursued in the design of the new metal containing polymer dielectrics to rapidly screen potential materials and provide a pathway to bypass the time-consuming process of carrying out numerous experimentations. By combining experimental data obtained here with DFT generated data, a better model can be devised to improve structure-property prediction for dielectric materials. This could then be expanded to other areas of materials discovery, in line with the objectives of the Materials Genome Initiative.

#### Acknowledgement

This work is supported through the Office of Naval Research grant (N00014-16-1-2580). The authors would like to acknowledge JoAnne Ronzello for her insightful suggestion and assisting in dielectric measurements and also Dr. Rui Ma for her initiative and valuable support.

#### Appendix A. Supplementary data

Supplementary data to this article can be found online at <https://doi.org/10.1016/j.polymer.2018.10.017>.

#### References

- [1] A. Mannodi-Kanakkithodi, G.M. Treich, T.D. Huan, R. Ma, M. Tefferi, Y. Cao, G.A. Sotzing, R. Ramprasad, Rational Co-design of polymer dielectrics for energy storage, *Adv. Mater.* (2016) 6277–6291, <https://doi.org/10.1002/adma.201600377>.
- [2] Materials Genome Initiative (MGI), (2011). <https://www.whitehouse.gov/mgi>.
- [3] T.D. Huan, S. Boggs, G. Teyssedre, C. Laurent, M. Cakmak, S. Kumar, R. Ramprasad, Advanced polymeric dielectrics for high energy density applications, *Prog. Mater.*

- Sci. 83 (2016) 236–269, <https://doi.org/10.1016/j.pmatsci.2016.05.001>.
- [4] T.D. Huan, A. Mannodi-Kanakkithodi, C. Kim, V. Sharma, G. Pilania, R. Ramprasad, A polymer dataset for accelerated property prediction and design, *Sci. Data*. 3 (2016) 160012, <https://doi.org/10.1038/sdata.2016.12>.
- [5] A. Mannodi-Kanakkithodi, C.C. Wang, R. Ramprasad, Compounds based on Group 14 elements: building blocks for advanced insulator dielectrics design, *J. Mater. Sci.* 50 (2014) 801–807, <https://doi.org/10.1007/s10853-014-8640-2>.
- [6] A. Mannodi-Kanakkithodi, T.D. Huan, R. Ramprasad, Mining materials design rules from data: the example of polymer dielectrics, *Chem. Mater.* 29 (2017) 9001–9010, <https://doi.org/10.1021/acs.chemmater.7b02027>.
- [7] W.J. Sarjeant, J. Zirnheld, F.W. MacDougall, Capacitors, *IEEE Trans. Plasma Sci.* 26 (1998) 1368–1392, <https://doi.org/10.1109/27.736020>.
- [8] Q. Chen, Y. Shen, S. Zhang, Q.M. Zhang, Polymer-based dielectrics with high energy storage density, *Annu. Rev. Mater. Res.* 45 (2015) 433–458, <https://doi.org/10.1146/annurev-matsci-070214-021017>.
- [9] J. Ho, T.R. Jow, S. Boggs, Historical introduction to capacitor technology, *IEEE Electr. Insul. Mag.* 26 (2010) 20–25, <https://doi.org/10.1109/MEL.2010.5383924>.
- [10] M.T. Sebastian, H. Jantunen, Low loss dielectric materials for LTCC applications: a review, *Int. Mater. Rev.* 53 (2008) 57–90, <https://doi.org/10.1179/174328008X277524>.
- [11] S. Tong, B. Ma, M. Narayanan, S. Liu, R. Koritala, U. Balachandran, D. Shi, Lead lanthanum zirconate titanate ceramic thin films for energy storage, *ACS Appl. Mater. Interfaces* 5 (2013) 1474–1480, <https://doi.org/10.1021/am302985u>.
- [12] R.G. Lorenzini, G.A. Sotzing, Furan/imide diels-alder polymers as dielectric materials, *J. Appl. Polym. Sci.* 131 (2014) 1–5, <https://doi.org/10.1002/app.40179>.
- [13] R. Ma, V. Sharma, A.F. Baldwin, M. Tefferi, I. Offenbach, M. Cakmak, Y. Cao, R. Ramprasad, G.A. Sotzing, Rational design and synthesis of polythioureas as capacitor dielectrics, *J. Mater. Chem.* (2015) 1–8, <https://doi.org/10.1039/C5TA01252J>.
- [14] V. Sharma, C. Wang, R.G. Lorenzini, R. Ma, Q. Zhu, D.W. Sinkovits, G. Pilania, A.R. Oganov, S. Kumar, G.A. Sotzing, S.A. Boggs, R. Ramprasad, Rational design of all organic polymer dielectrics, *Nat. Commun.* 5 (2014) 4845, <https://doi.org/10.1038/ncomms5845>.
- [15] T. Zhang, W. Huang, N. Zhang, T. Huang, J. Yang, Y. Wang, Grafting of polystyrene onto reduced graphene oxide by emulsion polymerization for dielectric polymer composites: high dielectric constant and low dielectric loss tuned by varied grafting amount of polystyrene, *Eur. Polym. J.* 94 (2017) 196–207, <https://doi.org/10.1016/j.eurpolymj.2017.07.008>.
- [16] N. González, M.D. Custal, G.N. Tomara, G.C. Psarras, J.-R. Riba, E. Armelin, Dielectric response of vulcanized natural rubber containing BaTiO<sub>3</sub> filler: the role of particle functionalization, *Eur. Polym. J.* 97 (2017) 57–67, <https://doi.org/10.1016/j.eurpolymj.2017.10.001>.
- [17] N. Madusanka, S.G. Shivareddy, M.D. Eddleston, P. Hiralal, R.A. Oliver, G.A.J. Amaratunga, Dielectric behaviour of montmorillonite/cyanohydrated cellulose nanocomposites, *Carbohydr. Polym.* 172 (2017) 315–321, <https://doi.org/10.1016/j.carbpol.2017.05.057>.
- [18] M.-S. Zheng, J.-W. Zha, Y. Yang, C.-Q. Li, P. Han, C.-H. Hu, Y.-Q. Wen, Z.-M. Dang, Ductile polymer-based films with ultrahigh permittivity and low dielectric loss, *Polymer* 130 (2017) 258–266, <https://doi.org/10.1016/j.polymer.2017.10.026>.
- [19] D. Xiang, L. Liu, Y. Liang, Effect of hard segment content on structure, dielectric and mechanical properties of hydroxyl-terminated butadiene-acrylonitrile copolymer-based polyurethane elastomers, *Polymer* 132 (2017) 180–187, <https://doi.org/10.1016/j.polymer.2017.11.001>.
- [20] B. Notario, J. Pinto, R. Verdejo, M.A. Rodríguez-Pérez, Dielectric behavior of porous PMMA: from the micrometer to the nanometer scale, *Polymer* 107 (2016) 302–305, <https://doi.org/10.1016/j.polymer.2016.11.030>.
- [21] M.S. Gaur, A.P. Indolia, Thermally stimulated dielectric properties of polyvinylidene fluoride-zinc oxide nanocomposites, *J. Therm. Anal. Calorim.* 103 (2011) 977–985, <https://doi.org/10.1007/s10973-010-1190-1>.
- [22] D. Vaishnav, R.K. Goyal, Thermal and dielectric properties of high performance polymer/ZnO nanocomposites, *IOP Conf. Ser. Mater. Sci. Eng.* 64 (2014) 012016, <https://doi.org/10.1088/1757-899X/64/1/012016>.
- [23] T.S. Velayutham, W.H. Abd Majid, W.C. Gan, A. Khorsand Zak, S.N. Gan, Theoretical and experimental approach on dielectric properties of ZnO nanoparticles and polyurethane/ZnO nanocomposites, *J. Appl. Phys.* 112 (2012), <https://doi.org/10.1063/1.4749414>.
- [24] Z.M. Dang, L.Z. Fan, S.J. Zhao, C.W. Nan, Preparation of nanosized ZnO and dielectric properties of composites filled with nanosized ZnO, *Mater. Sci. Eng. B Solid-State Mater. Adv. Technol.* 99 (2003) 386–389, [https://doi.org/10.1016/S0921-5107\(02\)00479-8](https://doi.org/10.1016/S0921-5107(02)00479-8).
- [25] D.F. Crisler, J.J. Cupal, A. R. Moore, Dielectric, piezoelectric, and electromechanical coupling constants of zinc oxide crystals, *Proc. IEEE* 56 (1968) 225–226, <https://doi.org/10.1109/PROC.1968.6246>.
- [26] N. Ashkenov, B.N. Mbenkum, C. Bundesmann, V. Riede, M. Lorenz, D. Spemann, E.M. Kaidashev, A. Kasic, M. Schubert, M. Grundmann, G. Wagner, H. Neumann, V. Darakchieva, H. Arwin, B. Monemar, Infrared dielectric functions and phonon modes of high-quality ZnO films, *J. Appl. Phys.* 93 (2003) 126–133, <https://doi.org/10.1063/1.1526935>.
- [27] S. Shit, A. Layek, Temperature dependent growth of cadmium(II) oxide nanocrystals: studies on morphology based optical, electrical and dielectric properties, *J. Mater. Sci. Mater. Electron.* 27 (2016) 3435–3442, <https://doi.org/10.1007/s10854-015-4176-8>.
- [28] S.K. Vasheghani Farahani, V. Muñoz-Sanjosé, J. Zúñiga-Pérez, C.F. McConville, T.D. Veal, Temperature dependence of the direct bandgap and transport properties of CdO, *Appl. Phys. Lett.* 102 (2013) 1–5, <https://doi.org/10.1063/1.4775691>.
- [29] P. Barber, S. Balasubramanian, Y. Anguchamy, S. Gong, A. Wibowo, H. Gao, H.J. Ploehn, H.C. Zur Loye, Polymer Composite and Nanocomposite Dielectric Materials for Pulse Power Energy Storage, (2009), <https://doi.org/10.3390/ma2041697>.
- [30] A.F. Baldwin, R. Ma, A. Mannodi-Kanakkithodi, T.D. Huan, C. Wang, M. Tefferi, J.E. Marszalek, M. Cakmak, Y. Cao, R. Ramprasad, G.A. Sotzing, Poly(dimethyltin glutarate) as a prospective material for high dielectric applications, *Adv. Mater.* 27 (2015) 346–351, <https://doi.org/10.1002/adma.201404162>.
- [31] A.F. Baldwin, R. Ma, T.D. Huan, Y. Cao, R. Ramprasad, G.A. Sotzing, Effect of incorporating aromatic and chiral groups on the dielectric properties of poly(dimethyltin esters), *Macromol. Rapid Commun.* 35 (2014) 2082–2088, <https://doi.org/10.1002/marc.201400507>.
- [32] G. Mannodi-Kanakkithodi, Pilania Arun, L.A. National, Scoping the polymer genome: a roadmap for rational polymer dielectrics design and beyond, *Mater. Today xxx* (2017), <https://doi.org/10.1016/j.matmod.2017.11.021>.
- [33] G.M. Treich, S. Nasreen, A. Mannodi-Kanakkithodi, R. Ma, M. Tefferi, J. Flynn, Y. Cao, R. Ramprasad, G.A. Sotzing, Optimization of organotin polymers for dielectric applications, *ACS Appl. Mater. Interfaces* (2016), <https://doi.org/10.1021/acsami.6b04091>.
- [34] W. Hohenberg, P. Kohn, P. Hohenberg, W. Kohn, *Phys. Rev.* 136 (1964) B864–B871, <https://doi.org/10.1103/PhysRev.136.B864>.
- [35] G. Kresse, J. Hafner, Ab initio molecular dynamics for liquid metals, *Phys. Rev. B* 47 (1993) 558–561, <https://doi.org/10.1103/PhysRevB.47.558>.
- [36] K. Lee, É.D. Murray, L. Kong, B.I. Lundqvist, D.C. Langreth, Higher-accuracy van der Waals density functional, *Phys. Rev. B* 82 (2010) 081101, <https://doi.org/10.1103/PhysRevB.82.081101>.
- [37] E.D. Murray, K. Lee, D.C. Langreth, Investigation of exchange energy density functional accuracy for interacting molecules, *J. Chem. Theor. Comput.* 5 (2009) 2754–2762, <https://doi.org/10.1021/ct900365q>.
- [38] C.S. Liu, G. Pilania, C. Wang, R. Ramprasad, How critical are the van der Waals interactions in polymer crystals? *J. Phys. Chem.* 116 (2012) 9347–9352, <https://doi.org/10.1021/jp3005844>.
- [39] H. Monkhorst, J. Pack, Special points for Brillouin zone integrations, *Phys. Rev. B* 13 (1976) 5188–5192, <https://doi.org/10.1103/PhysRevB.13.5188>.
- [40] R. Liang, F. Yue, Y. Wang, Y. Guo, X. Xuan, Syntheses, structures and fluorescence properties of cadmium coordination polymers with triangular 1,3-bis[2-(4'-pyridyl) ethenyl]benzene and linear dicarboxylic acids, *J. Mol. Struct.* 1119 (2016) 301–307, <https://doi.org/10.1016/j.molstruc.2016.04.067>.
- [41] X. Wang, C. Qin, E. Wang, Y. Li, N. Hao, C. Hu, L. Xu, Syntheses, structures, and photoluminescence of a novel class of d10 metal complexes constructed from pyridine-3,4-dicarboxylic acid with different coordination architectures, *Inorg. Chem.* 43 (2004) 1850–1856, <https://doi.org/10.1021/ic035151s>.
- [42] J. Wang, J.-Q. Tao, X.-J. Xu, C.-Y. Tan, Synthesis, crystal structure, and properties of a cadmium(II) complex with the flexible ligand (1'H-[2,2']Biimidazolyl-1-yl)-acetic acid, *Z. Anorg. Allg. Chem.* 638 (2012) 1261–1264, <https://doi.org/10.1002/zaac.201200043>.
- [43] B. Xu, J. Xie, H.M. Hu, X. Le Yang, F.X. Dong, M.L. Yang, G.L. Xue, Synthesis, crystal structure, and luminescence of Zn/Cd coordination polymers with a new functionalized terpyridyl carboxylate ligand, *Cryst. Growth Des.* 14 (2014) 1629–1641, <https://doi.org/10.1021/cg4016977>.
- [44] W. Marjit Singh, B.R. Jali, B. Das, J.B. Baruah, Synthesis, characterization, and reactivity of zinc carboxylate complexes of 2,3-pyridine dicarboxylic acid and (3-oxo-2,3-dihydro-benzo[1,4]oxazin-4-yl) acetic acid, *Inorg. Chim. Acta.* 372 (2011) 37–41, <https://doi.org/10.1016/j.ica.2010.08.045>.
- [45] P. Roy, Synthesis, characterization, and fluorescence properties of dinuclear cadmium(II) complexes, *J. Coord. Chem.* 62 (2009) 2003–2011, <https://doi.org/10.1080/00958970902751888>.
- [46] A. Kreider-Mueller, P.J. Quinlivan, J.S. Owen, G. Parkin, Synthesis and structures of cadmium carboxylate and thiocarboxylate compounds with a sulfur-rich coordination environment: carboxylate exchange kinetics involving tris(2-mercapto-1-t-butylimidazolyl)hydroborate cadmium complexes, [TmBut]Cd(O<sub>2</sub>CR), *Inorg. Chem.* 54 (2015) 3835–3850, <https://doi.org/10.1021/acs.inorgchem.5b00017>.
- [47] M. Dakanali, E.T. Kefalas, C.P. Raptopoulou, A. Terzis, T. Mavromoustakos, A. Salifoglou, Synthesis and spectroscopic and structural studies of a new cadmium(II)-citrate aqueous complex. Potential relevance to cadmium(II)-citrate speciation and links to cadmium toxicity, *Inorg. Chem.* 42 (2003) 2531–2537, <https://doi.org/10.1021/ic0205029>.
- [48] M. Amsler, S. Goedecker, Crystal structure prediction using the minima hopping method, *J. Chem. Phys.* 133 (2010), <https://doi.org/10.1063/1.3512900>.
- [49] M. Amsler, S. Botti, M.A.L. Marques, S. Goedecker, Conducting boron sheets formed by the reconstruction of the -boron (111) surface, *Phys. Rev. Lett.* 111 (2013), <https://doi.org/10.1103/PhysRevLett.111.136101>.
- [50] S. Baroni, S. De Gironcoli, A. Dal Corso, P. Giannozzi, Phonons and related crystal properties from density-functional perturbation theory, *Rev. Mod. Phys.* 73 (2001) 515–562, <https://doi.org/10.1103/RevModPhys.73.515>.
- [51] C.C. Wang, G. Pilania, R. Ramprasad, Dielectric properties of carbon-, silicon-, and germanium-based polymers: a first-principles study, *Phys. Rev. B* 87 (2013) 035103, <https://doi.org/10.1103/PhysRevB.87.035103>.
- [52] V. Peruzzo, G. Plazzogna, G. Tagliavini, The preparation and properties of some allyl tin carboxylates: R<sub>3</sub>SnOOCR' (R' = CH<sub>3</sub>, CH<sub>2</sub>Cl), R<sub>2</sub>Sn(OOCR')<sub>2</sub> (R' = CH<sub>2</sub>Cl, CHCl<sub>2</sub>) and [R<sub>2</sub>Sn(OOCR')]<sub>2</sub>O (R' = CH<sub>2</sub>Cl, CHCl<sub>2</sub>, CCl<sub>3</sub>), *J. Organomet. Chem.* 40 (1972) 129–133, [https://doi.org/10.1016/S0022-328X\(00\)86995-8](https://doi.org/10.1016/S0022-328X(00)86995-8).
- [53] K. Sowri Babu, A.R. Reddy, C. Sujatha, K.V. Reddy, A.N. Mallika, Synthesis and optical characterization of porous ZnO, *J. Adv. Ceram.* 2 (2013) 260–265, <https://doi.org/10.1007/s40145-013-0069-6>.
- [54] M. Ristic, S. Popovic, S. Music, Formation and properties of Cd(OH)<sub>2</sub> and CdO particles, *Mater. Lett.* 58 (2004) 2494–2499, <https://doi.org/10.1016/j.matlet.2004.05.001>.

- 2004.03.016.
- [55] E.G. Palacios, G. Juarez-Lopez, A.J. Monhemius, Infrared spectroscopy of metal carboxylates: II. Analysis of Fe(III), Ni and Zn carboxylate solutions, *Hydrometallurgy* 72 (2004) 139–148, [https://doi.org/10.1016/S0304-386X\(03\)00137-3](https://doi.org/10.1016/S0304-386X(03)00137-3).
- [56] E.V. Brusau, J.C. Pedregosa, G.E. Narda, G. Pozzi, G. Echeverria, G. Punte, Coordination binding modes for polymeric cadmium dicarboxylate hydrate complexes, *J. Coord. Chem.* 54 (2001) 469–480, <https://doi.org/10.1080/00958970108022657>.
- [57] M.S. Refat, D.N. Kumar, R.F. De Farias, Spectroscopic and thermal investigations of Cu(II), Zn(II), Cd(II), Pb(II) and Al(III) caproates, *J. Coord. Chem.* 59 (2006) 1857–1871, <https://doi.org/10.1080/00958970600662932>.
- [58] A.F. Baldwin, T.D. Huan, R. Ma, A. Mannodi-Kanakithodi, M. Tefferi, N. Katz, Y. Cao, R. Ramprasad, G.A. Sotzing, Rational design of organotin polyesters, *Macromolecules* 48 (2015) 2422–2428, <https://doi.org/10.1021/ma502424r>.
- [59] A. Erxleben, Structures and properties of Zn(II) coordination polymers, *Coord. Chem. Rev.* 246 (2003) 203–228, [https://doi.org/10.1016/S0010-8545\(03\)00117-6](https://doi.org/10.1016/S0010-8545(03)00117-6).
- [60] A. Synthesis, P. Pr, C. Oh, O. Clo, C. Kimblin, G. Parkin, C.I.B. Chemistry, Comparison of Zinc and Cadmium Coordination Environments in Synthetic Analogues of Carbonic Anhydrase (CA) Is the Zinc Enzyme Responsible for Equilibrating Bicarbonate with Carbon Dioxide and Water in Both Plants and Animals. 1 it Is, *Therefo*, (1996), pp. 6912–6913 1669.
- [61] S. Jana, S. Garain, S. Sen, D. Mandal, The influence of hydrogen bonding on the dielectric constant and the piezoelectric energy harvesting performance of hydrated metal salt mediated PVDF films, *Phys. Chem. Chem. Phys.* 17 (2015) 17429–17436, <https://doi.org/10.1039/c5cp01820j>.
- [62] R.G. Lorenzini, W.M. Kline, C.C. Wang, R. Ramprasad, G.A. Sotzing, The rational design of polyurea & polyurethane dielectric materials, *Polymer* 54 (2013) 3529–3533, <https://doi.org/10.1016/j.polymer.2013.05.003>.
- [63] Y. Ohki, N. Fuse, T. Arai, Band gap energies and localized states in several insulating polymers estimated by optical measurements, *Annu. Rep. - Conf. Electr. Insul. Dielectr. Phenomena, CEIDP*, 2010, <https://doi.org/10.1109/CEIDP.2010.5723991> 0–3.
- [64] P.P. González-Borrero, F. Sato, A.N. Medina, M.L. Baesso, A.C. Bento, G. Baldissera, C. Persson, G.A. Niklasson, C.G. Granqvist, A. Ferreira Da Silva, Optical band-gap determination of nanostructured WO<sub>3</sub> film, *Appl. Phys. Lett.* 96 (2010), <https://doi.org/10.1063/1.3313945>.
- [65] Z.M. Zaki, G.G. Mohamed, Spectral and thermal studies of thiobarbituric acid complexes, *Spectrochim. Acta. A. Mol. Biomol. Spectrosc.* 56A (2000) 1245–1250 <http://www.ncbi.nlm.nih.gov/pubmed/10888428>.
- [66] C. Zou, J.C. Fothergill, S.W. Rowe, The effect of water absorption on the dielectric properties of epoxy nanocomposites, *Dielectr. Electr. Insul. IEEE Trans.* 15 (2008) 106–117, <https://doi.org/10.1109/T-DEL.2008.4446741>.
- [67] J. Beuhler Allyson, R. Nowicki Neal, M. Gaudette Joanne, Dielectric characterization of water in polyimide and poly(amide?imide) thin films, *Polym. Mater. Electron. Packag. Interconnect*, 1989, pp. 67–76, , <https://doi.org/10.1021/bk-1989-0407.ch005>.